Nonlinear Band Expansion and 3D Nonnegative Tensor Factorization for Blind Decomposition of Magnetic Resonance Image of the Brain

Ivica Kopriva[1] and Andrzej Cichocki[2,3]

[1] Rudjer Bošković Institute, Bijenička cesta 54, P.O. Box 180, 10002, Zagreb, Croatia
[2] Laboratory for Advanced Brain Signal Processing
Brain Science Institute, RIKEN, Saitama, 351-0198, Japan
[3] Warsaw University of Technology and Systems Research Institute, PAN, Poland
ikopriva@irb.hr, cia@brain.riken.jp

Abstract. α- and β-divergence based nonnegative tensor factorization (NTF) is combined with nonlinear band expansion (NBE) for blind decomposition of the magnetic resonance image (MRI) of the brain. Concentrations and 3D tensor of spatial distributions of brain substances are identified from the Tucker3 model of the 3D MRI tensor. NBE enables to account for the presence of more brain substances than number of bands and, more important, to improve conditioning of the expanded matrix of concentrations of brain substances. Unlike matrix factorization methods NTF preserves local spatial structure in the MRI. Unlike ICA-, NTF-based factorization is insensitive to statistical dependence among spatial distributions of brain substances. Efficiency of the NBE-NTF algorithm is demonstrated over NBE-ICA and NTF-only algorithms on blind decomposition of the realistically simulated MRI of the brain.

Keywords: Nonnegative tensor factorization, nonlinear band expansion, magnetic resonance image, multi-spectral image.

1 Introduction

Blind or unsupervised multi-spectral and hyper-spectral image (MSI&HSI) decomposition attracts increased attention due to its capability to discriminate materials present in the MSI/HSI without knowing their spectral profiles [1]. For the purpose of blind decomposition, MSI is commonly represented in a form of the linear mixture model (LMM), whereupon vectorized version of the MSI is modeled as a product of the basis matrix, also known as spectral reflectance matrix, and matrix of vectorized spatial distributions of the materials present in the MSI, [1,2]. Magnetic resonance image (MRI) samples are images acquired by pulse sequences specified by three MR tissue parameters, spin-lattice (T_1) and spin-spin (T_2) relaxation times, and proton density (PD), [3,4]. Although MRI has different physical interpretation than MSI, it can also be represented using LMM, [3], and an analogy can be made with the three spectral MSI, such as red-green-blue (RGB) image, [5-7]. Here, basis matrix is interpreted as matrix of concentrations of the brain substances and source matrix represents vectorized spatial distributions of the brain substance present in the MRI. Each of the three

modalities of the MRI is designed for enhancing contrast of specific substance: PD for gray matter (GM), T_1 for white matter (WM) and T_2 for cerebral fluid (CF). Yet, each modality image still contains visible remnants of other substances, [3,4]. This appears to be especially true for PD image. Therefore, there is a need for additional (blind) post-processing (decomposition) of the acquired MRI.

Thanks to equivalence of the representations, advanced algorithms developed for the MSI data analysis can in principle be used for MRI analysis as well. In this paper we are particularly interested in blind decomposition methods due to their capabilities to estimate concentrations and spatial distributions of the brain substances having at disposal acquired MRI only. A standard tool for the solution of the related blind source separation (BSS) problem is independent component analysis (ICA), [8], which is based upon assumption that spatial distributions of the brain substances are non-Gaussian and statistically independent. However, as shown in [9,10], statistical independence assumption is not fulfilled for the hyper-spectral and multi-spectral data due to the fact that sum of the materials present in the pixel footprint must be constant. Thus, materials must necessarily be statistically related. Violation of statistical independence assumption is greater when dimensionality (number of spectral bands) of MSI is low, [6], which is also the case with 3-band MRI. Therefore, an algorithm for blind decomposition of the MRI the performance of which does not depend on statistical relations among brain substances is of great interest.

One avenue of research is related to algorithms that rely on sparseness between spatial distributions of the brain substances. The sparseness assumption implies that only small number of substances occupies each pixel footprint. Sparseness-based methodology has been applied in [5] for the purpose of blind decomposition of low-dimensional MSI and it is known as sparse component analysis (SCA), [11]. In this paper we rely on tensor representation of the MRI. As opposed to matrix representation, employed by ICA, SCA and/or nonnegative matrix factorization (NMF) algorithms, tensor representation preserves local spatial structure in the MRI. The main contribution of this manuscript is new method for blind decomposition of the 3-band MRI of the brain that combines nonlinear band expansion (NBE) and nonnegative tensor factorization (NTF). NBE has been used previously for blind MRI decomposition in combination with ICA in [3], and for blind MSI decomposition in combination with ICA and dependent component analysis (DCA) in [6]. NTF has been also used recently in [7] for blind MSI decomposition. We are unaware of previous combined application of NBE and NTF for blind MRI or MSI decomposition. NBE-NTF decomposition brings two improvements in relation to matrix factorization decomposition schemes: (*i*) NBE enables to account for the presence of more brain substances than number of bands, [3], and, more important, to improve conditioning of the expanded matrix of concentrations of brain substances. This is important for contrast enhancement between substances with similar concentration profiles. This has been used in [6] for robust blind decomposition of the low-dimensional low-intensity multi-spectral fluorescent image of the basal cell carcinoma; (*ii*) unlike ICA-, NTF-based factorization is insensitive to statistical dependence among spatial distributions of brain substances.

2 Theory and Algorithm

2.1 **Magnetic Resonance Image and Linear Mixture Model**

In analogy with MSI, MRI is represented in a form of matrix-based LMM [1-4]:

$$\mathbf{X}_{(3)} \approx \mathbf{AS} \tag{1}$$

where $\mathbf{X}_{(3)} \in R_{0+}^{3 \times I_1 I_2}$ represents 3-mode unfolded version, [12], of the original MRI tensor $\underline{\mathbf{X}} \in R_{0+}^{I_1 \times I_2 \times 3}$ consisted of three (T1, T2 and PD weighted) images with the size of $I_1 \times I_2$ pixels. Here, R_{0+} is a real manifold with nonnegative elements. Columns of $\mathbf{A} \in R_{0+}^{3 \times J}$ represent concentrations of the J brain substances present in the MRI, while rows of $\mathbf{S} \in R_{0+}^{J \times I_1 I_2}$ represent spatial distributions of these substances. Thus, BSS methods can be applied to factorize MRI $\mathbf{X}_{(3)}$ for enhancing contrast of the brain substances, [1,3], in the same spirit as it has been done in MSI analysis, [1,2,5,6]. However, matrix factorization problem implied by LMM (1) has infinitely many solutions unless additional constraints are imposed on model variables $\mathbf{A}$ or $\mathbf{S}$ in (1). NMF algorithms mostly impose sparseness constraints on $\left\{ \mathbf{s}_j \right\}_{j=1}^{J}$, while ICA algorithms impose statistical independence constraints on $\left\{ \mathbf{s}_j \right\}_{j=1}^{J}$. Sparseness constraints imply that at each pixel location (i_1, i_2) only few object exists. In medical imaging applications where pixel footprint is small it is justified to assume that only one object occupies each pixel footprint. Following described interpretation of the LMM (1), it is easy to verify that concentration similarity of the sources $\mathbf{s}_m$ and $\mathbf{s}_n$ affects the condition number of the mixing matrix $\mathbf{A}$. This is because the corresponding column vectors $\mathbf{a}_m$ and $\mathbf{a}_n$ become close to collinear. As shown in [6], in the context of MSI analysis, in addition to deteriorate conditioning of the mixing matrix concentration similarity between the sources makes them also statistically dependent. Hence, fundamental requirement imposed by the ICA algorithms fails when sources have similar concentration profiles and this occurs increasingly more often when number of bands is small. To relax constraint-based requirements we adopt 3D tensor representation of the MRI, whereupon MRI tensor $\underline{\mathbf{X}}$ is represented in a form of Tucker3 model [12-14]:

$$\underline{\mathbf{X}} \approx \underline{\mathbf{G}} \times_1 \mathbf{A}^{(1)} \times_2 \mathbf{A}^{(2)} \times_3 \mathbf{A}^{(3)} \tag{2}$$

Here, $\underline{\mathbf{X}} \in R_{0+}^{I_1 \times I_2 \times 3}$, $\underline{\mathbf{G}} \in R_{0+}^{J \times J \times J}$ is core tensor, $\left\{ \mathbf{A}^{(n)} \in R_{0+}^{I_n \times J} \right\}_{n=1}^{3}$ are array factors and $\times_n$ denotes n-mode product of a tensor with a matrix $\mathbf{A}^{(n)}$. 3-mode unfolded version of tensor $\underline{\mathbf{X}}$ in (2) is:

$$\mathbf{X}_{(3)} \approx \mathbf{A}^{(3)} \mathbf{G}_{(3)} \left[\mathbf{A}^{(2)} \otimes \mathbf{A}^{(1)} \right]^{\mathrm{T}} \tag{3}$$

where '$\otimes$' denotes Kronecker's product and $\mathbf{G}_{(3)}$ represent 3-mode unfolded core tensor $\underline{\mathbf{G}}$. In direct comparison between (1) and (3) we arrive at:

$$\mathbf{A} \approx \mathbf{A}^{(3)}$$
$$\underline{\mathbf{S}} \approx \underline{\mathbf{G}} \times_1 \mathbf{A}^{(1)} \times_2 \mathbf{A}^{(2)} = \underline{\mathbf{X}} \times_3 \left(\mathbf{A}^{(3)} \right)^{\dagger} \tag{4}$$

where $\underline{\mathbf{S}} \in R_{0+}^{I_1 \times I_2 \times J}$ represents tensor of spatial distributions of J brain substances contained in MRI and '$\dagger$' denotes the Moore-Penrose pseudo-inverse. Thus, NTF-based blind decomposition of MRI yields both matrix of concentrations and tensor of spatial distributions of the brain substances present in the MRI.

2.2 Nonlinear Band Expansion

Although the GM, WM and CF brain substances are of the main interest in MRI analysis, possible presence of other substances such as muscle, skin, fat, etc. as signal sources can violate the fundamental condition required by majority the BSS methods: the number of sources J must be less than or equal to the number of measurements. In the case of MRI number of measurements equals number of bands that is 3. Thus, number of sources most likely exceeds number of bands. To overcome this limitation, NBE has been used in combination with ICA to perform blind decomposition of MRI, [3]. However, in regard to the NBE there are two important points still missed in [3]: (*i*) in addition to increasing number of measurements NBE also improves conditioning of the matrix of the concentrations of brain substances: $\mathbf{A}$. This has been discussed in [6] in the context of low-dimensional MSI decomposition and is important for enhancing contrast between substances with similar concentration profiles; (*ii*) after NBE, sources in expanded mixture model still remain statistically dependent. This deteriorates accuracy of the ICA-based decomposition. To partially neutralize this problem, DCA has been used in [6]. Here, we propose combined use of NBE and NTF to perform blind MRI decomposition for enhancing contrast of WM, GM and CF brain substances. Let $\left\{ \mathbf{X}_{i_3} \in R_{0+}^{I_1 \times I_2} \right\}_{i_3=1}^{3}$ be set of original band (T$_1$, T$_2$ and PD) MR images. Through NBE we introduce new sets of images, [3,6]: set of auto-correlated band images $\left\{ \mathbf{X}_{i_3}^2 \right\}_{i_3=1}^{3}$, and set of cross-correlated band images $\left\{ \mathbf{X}_{i_3} \mathbf{X}_{j_3} \right\}_{i_3=1, j_3=i_3+1}^{2,3}$. The 3-mode unfolded version of the NBE MRI is then obtained as:

$$\overline{\mathbf{X}}_{(3)} \approx \overline{\mathbf{A}} \overline{\mathbf{S}} \tag{5}$$

where $\overline{\mathbf{X}}_{(3)} \in R_{0+}^{9 \times I_1 I_2}$, $\overline{\mathbf{A}} \in R_{0+}^{9 \times \overline{J}}$ and $\overline{\mathbf{S}} \in R_{0+}^{\overline{J} \times I_1 I_2}$. Thus, original 3-band MRI is transformed into 9-band image containing: 3 original band images, 3 auto-correlated band images and 3 cross-correlated band images. We now assume that only one brain substance occupies each pixel footprint. It is then straightforward to show that extended source matrix $\overline{\mathbf{S}}$ in addition to original source images $\left\{ \mathbf{s}_j \right\}_{j=1}^{J}$ contains also their squares $\left\{ \mathbf{s}_j^2 \right\}_{j=1}^{J}$. Thus, $\overline{J} = 2J$. Now, the BSS requirement $J \le 3$ transforms into $J \le 4.5$. It is however even more important that $\overline{\mathbf{A}}$ in (5) is better conditioned than $\mathbf{A}$ in (1), [6]. This enhances contrast between brain substances with similar concentrations across T$_1$, T$_2$ and PD bands. Due to its insensitivity to statistical dependence

among the sources and preservation of the local spatial structure of the MRI, we apply NTF-based decomposition on NBE MRI. Therefore, NBE MRI is represented in a tensor format using Tucker3 model:

$$\underline{\overline{\mathbf{X}}} \approx \underline{\overline{\mathbf{G}}} \times_1 \overline{\mathbf{A}}^{(1)} \times_2 \overline{\mathbf{A}}^{(2)} \times_3 \overline{\mathbf{A}}^{(3)} \tag{6}$$

where $\underline{\overline{\mathbf{X}}} \in R_{0+}^{I_1 \times I_2 \times 9}$, $\underline{\overline{\mathbf{G}}} \in R_{0+}^{2J \times 2J \times 2J}$ is core tensor and $\left\{ \overline{\mathbf{A}}^{(n)} \in R_{0+}^{I_n \times 2J} \right\}_{n=1}^{3}$ are factors. 3-mode unfolded version of tensor $\underline{\overline{\mathbf{X}}}$ in (6) is:

$$\overline{\mathbf{X}}_{(3)} \approx \overline{\mathbf{A}}^{(3)} \overline{\mathbf{G}}_{(3)} \left[\overline{\mathbf{A}}^{(2)} \otimes \overline{\mathbf{A}}^{(1)} \right]^{\mathrm{T}} \tag{7}$$

where $\overline{\mathbf{G}}_{(3)}$ represent 3-mode unfolded core tensor $\underline{\overline{\mathbf{G}}}$. In direct comparison between (7) and (5) we obtain:

$$\overline{\mathbf{A}} \approx \overline{\mathbf{A}}^{(3)}$$
$$\underline{\overline{\mathbf{S}}} \approx \underline{\overline{\mathbf{G}}} \times_1 \overline{\mathbf{A}}^{(1)} \times_2 \overline{\mathbf{A}}^{(2)} = \underline{\overline{\mathbf{X}}} \times_3 \left(\overline{\mathbf{A}}^{(3)} \right)^{\dagger} \tag{8}$$

where $\underline{\overline{\mathbf{S}}} \in R_{0+}^{I_1 \times I_2 \times 2J}$. Improved conditioning of $\overline{\mathbf{A}}^{(3)}$ is of great importance for increasing accuracy of the NBE-NTF-based decomposition because its pseudo-inverse is involved in calculation of the expanded tensor of spatial distributions of brain substances $\underline{\overline{\mathbf{S}}}$.

3   Experiment

MRI used for comparative performance analysis was obtained from the MRI simulator of McGill University, [15,16]. Three MR images of the brain corresponding to modalities PD, T_1 and T_2 are obtained under the following specifications: protocol=International Consortium of Brain Mapping (ICBM), phantom name=normal, slice thickness=5 mm, noise=0%, INU=0%. Generated volume contained 36 MR image slices in Z direction with a size of each slice of 217×181 pixels. We have used MRI slice number 13 to demonstrate NBE-NTF-, NBE-ICA- and NTF-based blind MRI decompositions. Implementations of Tucker3 α- and β-NTF algorithms, [12,13], were based on MATLAB Tensor Toolbox provided at [17]. For ICA-based decompositions enhanced version (EFICA), [18], of the FastICA algorithm with *tanh* nonlinearity has been used. Efficiency of NBE-NTF decomposition of the MRI image against NBE-ICA and NTF decompositions is demonstrated on the synthetic brain images as in [3]. Figure 1 shows three simulated MR images of the brain with PD,
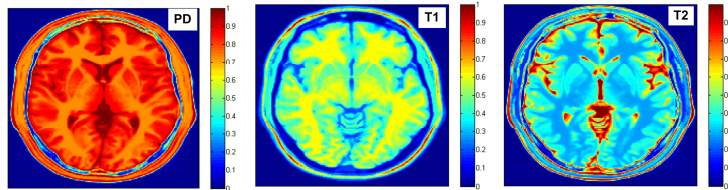

Fig. 1. (color online). Realistically simulated MRI of the brain from left to right: PD (GM), T_1 (WM) and T_2 (CF).

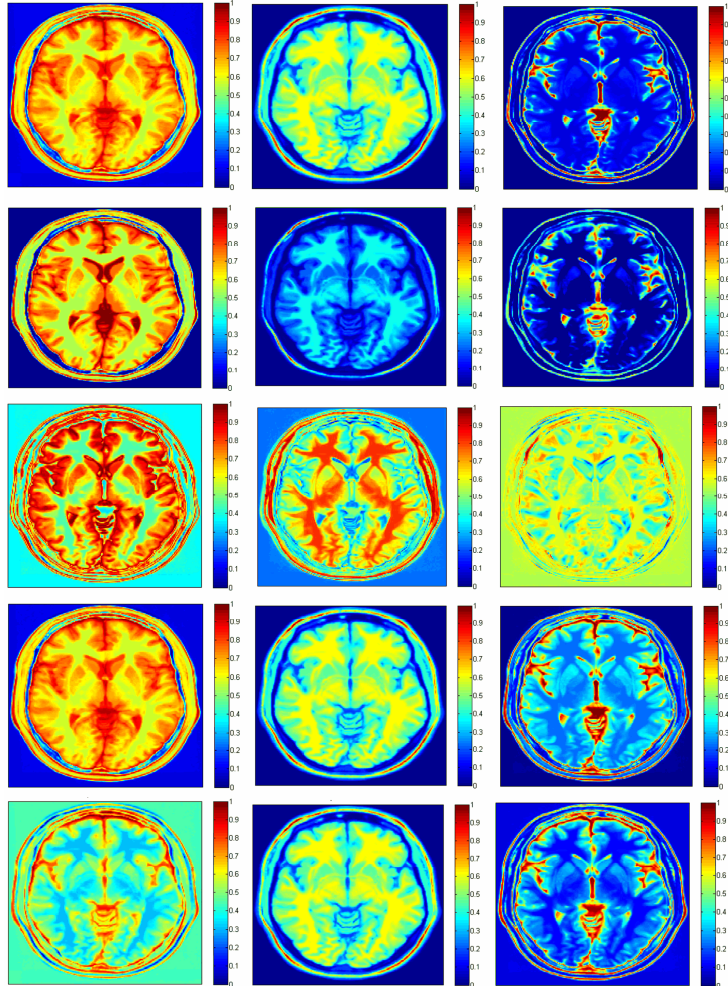**Fig. 2.** (color online). GM, WM and CF brain substance images obtained by, from top to bottom: NBE and α-NTF blind decomposition with α=2; NBE and β-NTF blind decomposition with β=1; NBE and EFICA algorithm with *tanh* nonlinearity; α-NTF algorithm with α=2; β-NTF algorithm with β=1. All NTF-based results are obtained after 5000 iterations.

T_1 and T_2 modalities. Comparative performance analysis is focused on the spatial distributions of GM, WM and CF because they are of actual interest in MRI. Thus, Figure 2 shows spatial distributions of GM, WM and CF brain substances extracted respectively by: NBE and Tucker3 α-NTF algorithm; NBE and Tucker3 β-NTF algorithm; NBE and EFICA algorithm; Tucker3 α-NTF algorithm, and Tucker3 β-NTF algorithm. Combined NBE and Tucker3 NTF takes approximately 5 minutes in MATLAB environment on PC running under the Windows XP operating system using Intel Core 2 Quad Processor Q6600 operating with clock speed of 2.4 GHz and 16GB of RAM installed. Images in Figures 1 and 2 are rescaled to interval [0,1] and
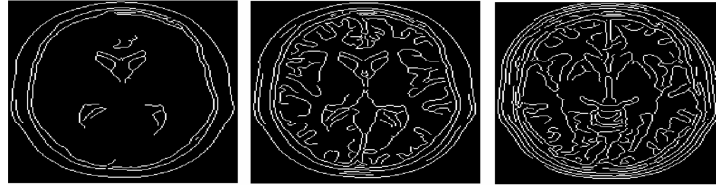
Fig. 3. From left to right: edges of the GM spatial map extracted by Canny's algorithm with a threshold set to 0.2 from original PD image, NBE and β-NTF segmented image and β-NTF only segmented image

shown in pseudo-color scale. Probability of substance presence 0 is shown in dark blue color and probability of substance presence 1 is shown in dark red color. Except rescaling to [0,1] interval no additional post-processing has been done on decomposition results shown in Figure 2. Binary maps of decomposed images could be easily obtained through intensity-based segmentation of decomposed images. α- and β-NBE-NTF algorithms extracted all three substances correctly, while NBE-ICA and α- and β-NTF algorithms failed to do so. NBE-ICA failed due to the violation of the statistical independence assumption. Worse performance of α- and β-NTF algorithms is caused by poorer conditioning of the matrix of concentrations that was caused by similarity of concentrations of brain substances. This is demonstrated in Figure 3 where edge maps extracted by Canny's algorithm with a threshold set to 0.2 are shown for GM substance obtained from original PD image, NBE and β-NTF obtained spatial map and β-NTF only obtained spatial map. Due to the poor contrast boundary edges were completely missed for original PD image, were better detected from β-NTF segmented image and even more better from NBE and β-NTF segmented image.

4   Conclusion

Following analogy with MSI, MRI of the brain is represented by LMM using Tucker3 model of the 3D MRI tensor. Matrix of the concentrations of brain substances is identified as mode-3 array factor of the 3D MRI tensor, while 3D tensor of spatial distributions of the brain substances is obtained through 3-mode tensor product between MRI tensor and pseudo-inverse of the mode-3 array factor. Tensor-based representation of the MRI preserves local spatial structure of the images and yields factorization insensitive to statistical dependence among the spatial distributions of the brain substances present in the MRI. To further improve accuracy of MRI decomposition, the MRI tensor is expanded through nonlinear band expansion yielding new MRI tensor with 9-bands (as opposed to original 3-band MRI). In relation to original MRI tensor, the band-expanded tensor is characterized with mode-3 array factor that is better conditioned which is important for enhancing contrast between brain substances with similar concentrations across T_1, T_2 and PD bands.

References

1. Chang, C.I. (ed.): Hyperspectral Data Exploitation: Theory and Applications, New York. John Wiley, Chichester (2007)
2. Du, Q., Kopriva, I., Szu, H.: Independent-component analysis for hyperspectral remote sensing imagery classification. Opt. Eng. 45, 1–13 (2006)
3. Ouyang, Y.C., Chen, H.M., Chai, J.W., Chen, C.C.C., Poon, S.K., Yang, C.W., Lee, S.K., Chang, C.I.: Band Expansion-Based Over-Complete Independent Component Analysis for Multispectral Processing of Magnetic Resonance Image. IEEE Trans. Biomed. Eng. 55, 1666–1677 (2008)
4. Nakai, T., Muraki, S., Bagarinao, E., Miki, Y., Takehara, Y., Matsuo, K., Kato, C., Sakahara, H., Isoda, H.: Application of independent component analysis to magnetic resonance imaging for enhancing the contrast of gray and white matter. Neuroimage 21, 251–260 (2004)
5. Kopriva, I., Cichocki, A.: Blind decomposition of low-dimensional multi-spectral image by sparse component analysis. J. Chemometrics 23, 590–597 (2009)
6. Kopriva, I., Peršin, A.: Unsupervised decomposition of low-intensity low-dimensional multi-spectral fluorescent images for tumour demarcation. Med. Image Analysis 13, 507–518 (2009)
7. Kopriva, I., Cichocki, A.: Blind Multi-spectral Image Decomposition by 3D Nonnegative Tensor Factorization. Opt. Lett. 34, 2210–2212 (2009)
8. Cichocki, A., Amari, S.: Adaptive Blind Signal and Image Processing. John Wiley, Chichester (2002)
9. Nascimento, J.M.P., Dias, J.M.B.: Does Independent Component Analysis Play a Role in Unmixing Hyperspectral Data? IEEE Trans. Geosci. Remote Sens. 43, 175–187 (2005)
10. Nascimento, J.M.P., Dias, J.M.B.: Vertex Component Analysis: A Fast Algorithm to Unmix Hyperspectral Data. IEEE Trans. Geosci. Remote Sens. 43, 898–910 (2005)
11. Li, Y., Cichocki, A., Amari, S.: Analysis of Sparse Representation and Blind Source Separation. Neural Comput. 16, 1193–1234 (2004)
12. Cichocki, A., Zdunek, R., Phan, A.H., Amari, S.I.: Nonnegative Matrix and Tensor Factorizations - Applications to Exploratory Multi-way Data Analysis and Blind Source Separation. John Wiley, Chichester (2009)
13. Cichocki, A., Phan, A.H.: Fast Local Algorithms for Large Scale Nonnegative Matrix and Tensor Factorizations. IEICE Trans. Fundamentals E92-A(3), 708–721 (2009)
14. Tucker, L.R.: Some mathematical notes on three-mode factor analysis. Psychometrika 31, 279–311 (1966)
15. Kwan, R.K.S., Evans, A.C., Pike, G.B.: MRI Simulation-Based Evaluation of Image-Processing and Classification Methods. IEEE Trans. Med. Imag. 18, 1085–1097 (1999)
16. http://www.bic.mni.mcgill.ca/brainweb/
17. http://csmr.ca.sandia.gov/~tkolda/TensorToolbox
18. Koldovský, Z., Tichavský, P., Oja, E.: Efficient Variant of Algorithm for FastICA for Independent Component Analysis Attaining the Cramér-Rao Lower Bound. IEEE Trans. Neural Net. 17, 1265–1277 (2006)